Pinching Antenna Systems versus Reconfigurable Intelligent Surfaces in mmWave

Mostafa Samy, *Graduate Student Member, IEEE*, Hayder Al-Hraishawi, *Senior Member, IEEE*, Madyan Alsenwi, *Member, IEEE*, Abuzar B. M. Adam, *Member, IEEE*, Symeon Chatzinotas, *Fellow, IEEE*, and Björn Otteresten, *Fellow, IEEE*

***Abstract*—Flexible and intelligent antenna designs, such as pinching antenna systems and reconfigurable intelligent surfaces (RIS), have gained extensive research attention due to their potential to enhance the wireless channels. This letter, for the first time, presents a comparative study between the emerging pinching antenna systems and RIS in millimeter wave (mmWave) bands. Our results reveal that RIS requires an extremely large number of elements (in the order of 10^4) to outperform pinching antenna systems in terms of spectral efficiency, which severely impact the energy efficiency performance of RIS. Moreover, pinching antenna systems demonstrate greater robustness against hardware impairments and severe path loss typically encountered in high-frequency mmWave bands.**

***Index Terms*—Pinching antenna systems, reconfigurable intelligent surfaces (RIS), millimeter wave (mmWave), spectral efficiency, energy efficiency.**

I. Introduction

The growing demand for ultra-high data rates for next-generation 6G wireless networks is driving the exploration of spectrum resources, in millimeter-wave (mmWave) bands [1]. Large bandwidths are available in mmWave and they are well-suited for supporting the increasing number of intelligent devices and latency-sensitive applications that require high data rates [2]. However, one of the fundamental challenges of mmWave communication is the severe path loss and susceptibility to blockages [3].

In light of this, reconfigurable intelligent surfaces (RIS) are envisioned to overcome link blockage in mmWave by reflecting signals around obstacles and providing virtual line-of-sight (LoS) connection between transceivers [2]. The RIS is typically comprised of a large number of low-cost, reconfigurable passive elements, where each element can manipulate the phase shift of an incident electromagnetic wave in a controlled manner, thus enabling a 'smart', i.e., programmable, wireless environment [4]. Despite such potential, RIS inherently suffers from double large-scale attenuation due to its passive nature, which becomes more severe at higher carrier frequencies such as mmWave, where wavelengths are shorter.

Recently, a new flexible-antenna technology, termed pinching antennas, has been proposed, a more promising solution to combat the large scale path loss, at higher propagation frequencies [5], [6]. The pinching antenna systems consist of a waveguide connected to a radio frequency (RF) source and small dielectric particles on the waveguide, such as plastic pinches, to enable the electromagnetic waves to radiate or be received through the pinching antenna [5]. Furthermore, the location of pinching antennas can be flexibly adjusted along a waveguide, enabling the creation or enhancement of LoS links [7]. Moreover, dielectric waveguides offer significantly lower propagation loss in high-frequency bands compared to free-space path loss. For instance, a high-purity Teflon-based dielectric waveguide exhibits a propagation loss of approximately 0.08 dB/m at 28 GHz, whereas the free-space path loss is around 40 dB/m [6].

In this direction, important research efforts have been made to assess the benefits of pinching antenna systems across various communication scenarios [6], [8]–[11]. For instance, the work in [6] theoretically characterized the ergodic rate achieved by pinching antennas and demonstrated their ability to deliver enhanced spectral performance compared to conventional fixed-position antenna systems. The authors in [8] and [9], optimized the locations of the pinching antennas for downlink and uplink scenarios, respectively. In [10], the authors investigated the activation of multiple pinching antennas to serve multiple users in non-orthogonal multiple access (NOMA) downlink scenario. Reference [11] jointly optimized the pinching antenna placement and user power allocation to enhance communication and sensing performance of integrated sensing and communication (ISAC) systems.

Despite this growing interest in exploring pinching antenna systems across various application scenarios in mmWave bands, to the best of the authors' knowledge, a comparative analysis with RIS technology has not been explored yet. As the first study to present such comparison, the primary goal of this letter is to identify the advantages and challenges associated with both technologies. Furthermore, hardware impairments for pinching antennas and RIS are incorporated to ensure a realistic comparison.

II. System Model

We consider a device-to-device communication scenario, that consists of two single-antenna users, denoted by U_k for $k \in \{1, 2\}$, operating in mmWave band. U_1 and U_2 aim to exchange data (e.g., file sharing), where the direct link between the two users is not available due to blockage. To overcome this, we consider two setups to assist the communication, as shown in Fig. 1: A pinching antenna system in Fig. 1(a), and

M. Samy, M. Alsenwi, A. B. M. Adam, and B. Otteresten are with the Interdisciplinary Centre for Security, Reliability and Trust (SnT), University of Luxembourg, Luxembourg.
H. Al-Hraishawi is with the Department of Electrical Engineering, University of South Florida, Tampa, FL 33620 USA.
S. Chatzinotas is with SnT, University of Luxembourg, 1855 Luxembourg City, Luxembourg and with College of Electronics & Information, Kyung Hee University, Yongin-si, 17104, Korea.
Corresponding author: *Mostafa Samy (mostafa.samy@uni.lu)*.

This work was supported by the Luxembourg National Research Fund (FNR) through the AFR Project CEP-MBD-CRIS, Grant reference 17974844.

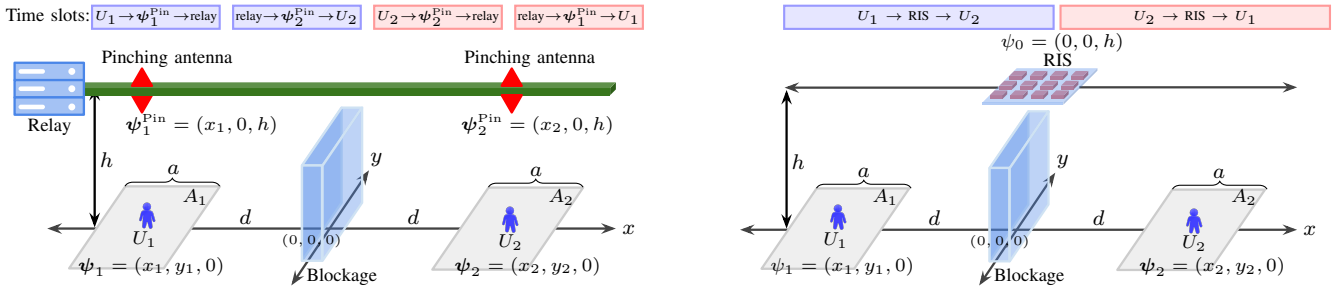

(a) Pinching antenna system: In each time slot, a single pinching antenna is activated to serve U_k during its transmission to or reception from the relay.

(b) RIS-assisted system: U_1 transmits in time slot 1, and U_2 transmits in time slot 2, with both transmissions facilitated by the RIS.

Fig 1. System model of device-to-device communication assisted by (a) pinching-antenna system and (b) RIS in the mmWave band.

RIS-assisted communication system in Fig. 1(b). We assume the service area of U_k is denoted by A_k and is assumed to be a square with side length denoted by a. The users are assumed to be uniformly distributed in A_k, and U_k's location is denoted by $\boldsymbol{\psi}_k = (x_k, y_k, 0)$. The distance from the origin to A_k is denoted by d.

A. Pinching Antenna System

In this setup, a waveguide is placed parallel to the x-axis at height h from the origin, and connected to a single RF chain relay, as illustrated in Fig. 1(a). We assume that a pinching antenna can be moved to the location closest to the served user, and hence, the location of the pinching antenna is $\boldsymbol{\psi}_k^{\text{Pin}} = (x_k, 0, h)$ [6]. In this communication scenario, the transmission is performed in four time slots[1]. In the first time slot, U_1 transmit the data to the relay using pinching antenna $\boldsymbol{\psi}_1^{\text{Pin}}$, and in the second time slot the relay transmit the signal to U_2 through pinching antenna $\boldsymbol{\psi}_2^{\text{Pin}}$. Similarly, in the third time slot, U_2 send its signal to the relay via $\boldsymbol{\psi}_2^{\text{Pin}}$, and in the fourth time slot, the relay retransmit the signal to U_1 via $\boldsymbol{\psi}_1^{\text{Pin}}$. The reason for not performing the communication directly in two time slots through the channel path U_1-$\boldsymbol{\psi}_1^{\text{Pin}}$-waveguide-$\boldsymbol{\psi}_2^{\text{Pin}}$-$U_2$ will be discussed later. We assume that the users' channel state information (CSI) is perfectly known at the relay, where CSI knowledge is crucial for positioning the pinching antenna [6]. Since pinching antennas effectively reduce the transceiver distance, where the likelihood of a LoS link increases as this distance shortens, free-space path loss model is considered [6]. For a fair comparison with the RIS-assisted communication scenario, we assume that the total transmit power allocated per user over its two time slots is P_k, meaning both U_k and the relay each transmit with power $\frac{P_k}{2}$. Hence, the received signal-to-noise-ratio (SNR) of U_k at the relay is given as:

$$\gamma_{rel,k}^{\text{Pin}} = \frac{P_k \eta}{2\sigma^2 |\boldsymbol{\psi}_{k'}^{\text{Pin}} - \boldsymbol{\psi}_{k'}|^2} = \frac{P_k \eta}{2\sigma^2 (h^2 + y_{k'}^2)}, \tag{1}$$

where $k' \neq k$ denotes the transmitting user. In (1), $\eta = \frac{c^2}{16\pi^2 f_c^2}$, c denotes the speed of light, f_c is the carrier frequency, σ^2 denotes the noise power. Similarly, the received SNR at user U_k, when the relay transmits with power $\frac{P_k}{2}$, is given by:

$$\gamma_k^{\text{Pin}} = \frac{P_k \eta}{2\sigma^2 |\boldsymbol{\psi}_k^{\text{Pin}} - \boldsymbol{\psi}_k|^2} = \frac{P_k \eta}{2\sigma^2 (h^2 + y_k^2)}. \tag{2}$$

[1]The considered system model is similar to conventional decode-and forward relaying in cooperative communication, however, implemented using a pinching antenna system.

Therefore, the average spectral efficiency for U_k is given as:

$$R_k^{\text{Pin}} = \mathbb{E}\left[\frac{1}{4}\log_2\left(1 + \min\left(\gamma_{rel,k}^{\text{Pin}}, \gamma_k^{\text{Pin}}\right)\right)\right], \tag{3}$$

where $\mathbb{E}[\cdot]$ is the expectation operator, and the pre-log factor is due to the use of four time slots for communication. Deriving a closed-form expression for (3) is challenging, which motivates the use of an upper bound. Assuming symmetric user locations (i.e., $y_1 = y_2$), the SNR expressions in (1) and (2) become equal. Hence, R_k^{Pin} can be obtained from [6] as follows:

$$R_k^{\text{Pin}} = \frac{1}{4}\left[\frac{4}{a}\log_2(e)\sqrt{h^2 + \frac{\eta P_k}{2\sigma^2}}\tan^{-1}\left(\frac{a}{2\sqrt{h^2 + \frac{\eta P_k}{\sigma^2}}}\right) - \log_2\left(\frac{a^2}{4} + h^2\right) + \log_2\left(\frac{a^2}{4} + h^2 + \frac{\eta P_k}{2\sigma^2}\right) - \frac{4}{a}\log_2(e) h \tan^{-1}\left(\frac{a}{2h}\right)\right], \tag{4}$$

where $\tan(\cdot)^{-1}$ denotes the inverse tangent function.

Remark: The system model shown in Fig. 1(a) suggests that the two users can communicate directly by simultaneously activating the two pinching antennas $\boldsymbol{\psi}_1^{\text{Pin}}$ and $\boldsymbol{\psi}_2^{\text{Pin}}$, i.e., through the channel path U_1-$\boldsymbol{\psi}_1^{\text{Pin}}$-waveguide-$\boldsymbol{\psi}_2^{\text{Pin}}$-$U_2$, where users exchange signals in two orthogonal time slots. At first glance, this communication scheme appears to offer enhanced spectral efficiency, which, however, is not true, as explained in the following. Considering this scenario, the SNR per user can be given as follows:

$$\gamma_k = \frac{\eta^2 P_k}{\sigma^2 |\boldsymbol{\psi}_1^{\text{Pin}} - \boldsymbol{\psi}_1|^2 |\boldsymbol{\psi}_2^{\text{Pin}} - \boldsymbol{\psi}_2|^2}, \tag{5}$$

which shows that the SNR includes a double path loss factor. In other words, the pinching antenna system is acting as a passive device in a manner similar to the RIS, which significantly increases signal attenuation[2]. We refer to this scheme as passive pinching antenna, which we also evaluate in the numerical section.

B. RIS-Assisted System

In this alternative setup, we assume a RIS comprising of M reflecting elements, for $M \in \{1, ..., M\}$, is deployed at a fixed location in the middle between the two users at hight h,

[2]Note that when considering hardware impairments, an additional waveguide path loss will be included to the power calculation of the link budget for this scheme. Hence, the total path loss in this scenario is the product of three components: from $\boldsymbol{\psi}_1$ to $\boldsymbol{\psi}_1^{\text{Pin}}$, waveguide path loss, and from $\boldsymbol{\psi}_2^{\text{Pin}}$ to $\boldsymbol{\psi}_2$.

i.e., positioned at $\boldsymbol{\psi}_0 = (0, 0, h)$, as shown in Fig. 1(b)[3]. In this scenario, communication takes place over two time slots, where each user U_k transmits its data to the other through the RIS in one of the slots. We model the RIS channels in the mmWave band using Rician fading[4], similar to [13], [14]. To ensure a fair comparison with the pinching antenna system, a dominant LoS (e.g., a Rician factor of 10) will be considered in the numerical results. In this case, we denote the small-scale fading channels from U_k to the RIS and from the RIS to $U_{k'}$ as $\mathbf{h} \in \mathbb{C}^{M\times 1}$ and $\mathbf{g} \in \mathbb{C}^{1\times M}$, respectively. These are expressed as follows:

$$\mathbf{h} = [h_1, \cdots h_m, \cdots, h_M]^{\mathrm{T}}, \text{and } \mathbf{g} = [g_1, \cdots, g_m, \cdots, g_M], \tag{6}$$

where $h_m = \delta_m e^{-j\upsilon_m}$ and $g_m = \zeta_m e^{-j\varrho_m}$ denote the fading coefficients of the incident and reflection channels of the m-th element, respectively. Further, δ_m and ζ_m are the channel amplitudes, while υ_m and ϱ_m are the phase shifts. All channels are assumed to be independent and identically distributed, and the Rician factor of the channels is denoted by $\mathcal{K}$. Therefore, the received SNR per user is given as follows:

$$\gamma_k^{\mathrm{RIS}} = \frac{P_k |\sum_{m=1}^{M} \delta_m \zeta_m e^{-j(\theta_m+\upsilon_m+\varrho_m)}|^2}{\sigma^2 \mathscr{L}_1(|\boldsymbol{\psi}_0 - \boldsymbol{\psi}_1|)\mathscr{L}_2(|\boldsymbol{\psi}_0 - \boldsymbol{\psi}_2|)}, \tag{7}$$

where θ_m denotes the phase shift introduced by the m-th RIS element. In (7), $\mathscr{L}_k(|\boldsymbol{\psi}_0 - \boldsymbol{\psi}_k|)$ is the path loss between U_k and the RIS that is function of the distance in-between. We adopt the widely used Saleh-Valenzuela (SV) channel model [13], [14] for modeling both links as follows:

$$\mathscr{L}_k^{[\mathrm{dB}]}(|\boldsymbol{\psi}_0 - \boldsymbol{\psi}_k|) = a + 10b\log_{10}(|\boldsymbol{\psi}_0 - \boldsymbol{\psi}_k|) + \xi, \tag{8}$$

where a is the path loss constant offset value, b is the path loss attenuation constant, and ξ is the shadow fading component with shadowing standard deviation set to $\sigma_{\mathrm{SF}} = 0$ [15]. After applying the coherent phase-shift design [4], i.e., setting $\theta_m = -(\upsilon_m + \varrho_m)$ in each user's time slot to maximize the channel gain, the SNR per user can be expressed as:

$$\gamma_k^{\mathrm{RIS}} = \frac{P_k |\sum_{m=1}^{M} \delta_m \zeta_m|^2}{\sigma^2 \mathscr{L}_1(\sqrt{x_1^2 + y_1^2 + h^2})\mathscr{L}_2(\sqrt{x_2^2 + y_2^2 + h^2})}. \tag{9}$$

Therefore, the average spectral efficiency can be obtained as

$$\mathcal{R}_k^{\mathrm{RIS}} = \mathbb{E}\left[\frac{1}{2}\log_2\left(1 + \gamma_k^{\mathrm{RIS}}\right)\right]. \tag{10}$$

By using Jensen's inequality, an upper bound of the spectral efficiency in (10) is given by

$$\mathcal{R}_k^{\mathrm{RIS}} \leq \tilde{\mathcal{R}} = \frac{1}{2}\log_2\left(1 + \mathbb{E}[\gamma_k^{\mathrm{RIS}}]\right). \tag{11}$$

The randomness in the SNR arises from the fading channels δ_m and ζ_m as well as the random user coordinates x_k and y_k. To facilitate a tractable analysis and derive a closed-form expression, we assume the users are located at the center of the coverage area A_k. Under this assumption, $\mathscr{L}_1(|\boldsymbol{\psi}_0 - \boldsymbol{\psi}_1|)$ and $\mathscr{L}_2(|\boldsymbol{\psi}_0 - \boldsymbol{\psi}_2|)$ become $\mathscr{L}\left(\sqrt{\left(d + \frac{a}{2}\right)^2 + h^2}\right)$. Hence, the spectral efficiency can be obtained in closed-form as follows:

$$\mathcal{R}_k^{\mathrm{RIS}} = \log_2\left(1 + \frac{P_k\left[M + \left(\frac{\pi^2 L_{\frac{1}{2}}(-\mathcal{K})^4}{16(\mathcal{K}+1)^2}\right)(M^2 - M)\right]}{\sigma^2 \mathscr{L}\left(\sqrt{\left(d + \frac{a}{2}\right)^2 + h^2}\right)^2}\right), \tag{12}$$

where $L_{\frac{1}{2}}(-\mathcal{K})$ is the Laguerre polynomial [16].

III. Energy Efficiency

This section analyzes the energy efficiency of pinching antenna and RIS systems by developing a power consumption model for the studied communication systems. The energy efficiency is defined as the ratio of the achievable data rate to the total power consumption of the system, measured in bits per joule (b/J), as follows:

$$EE = \frac{B \cdot \mathcal{R}^{\mathrm{sum}}}{\mathcal{P}_{\mathrm{tot}}}, \tag{13}$$

where B denotes the transmission bandwidth in Hz, $\mathcal{R}^{\mathrm{sum}}$ denotes the sum spectral efficiency achieved by the two users. $\mathcal{P}_{\mathrm{tot}}$ is the total power consumed by the whole communication system. In the following, we provide the energy efficiency analysis for the two communication scenarios.

A. Pinching Antenna System

Recall that, in the considered pinching antenna system, each user transmits with power $\frac{P_k}{2}$, while the relay transmits with a total power of P_k to serve both users. Define $\nu \in (0, 1]$ as the power amplifier efficiency of the relay [17]. We consider continuous activation, where a slide track is installed parallel to the waveguide, and a micro motor is employed to enable precise movement and positioning of the pinching antenna [18]. Inspired by the work in [19] for movable antenna technology, we assume the pinching antenna is driven by a stepper motor, which employs a timing belt as its linear actuator. To shorten the movement time, we consider a user-centric deployment approach [18], where each user is served by a pinching antenna in its service area. Hence, two stepper motors are used for each pinching antenna: One to enable linear movement along the service area for U_k, and another attached to the plastic pinch to perform the pinch/release action. Accordingly, the overall energy efficiency for the pinching antenna system can be given as follows:

$$EE^{\mathrm{Pin}} = \frac{B \cdot \sum_k^{K=2} R_k^{\mathrm{Pin}}}{P_k/\nu + P_{\mathrm{RE}} + \sum_k^{K=2}(P_k/2 + P_{\mathrm{UE},k} + P_{\mathrm{mov},k} + P_{\mathrm{pin},k})}, \tag{14}$$

where P_{RE} and $P_{\mathrm{UE},k}$ denote the static power consumption of the relay equipment and the user equipment, respectively. In (14), $P_{\mathrm{mov},k}$ and $P_{\mathrm{pin},k}$ represent the power consumed by the stepper motors responsible for linear movement and the pinch/release actions, respectively, for the pinching antenna of U_k. Similar to [19], we consider the high-speed stepper motor AM2224 for the linear motion [20]. Moreover, we consider a lighter stepper motor AM1020 attached to the plastic pinch to perform the pinch/release action [21].

[3]Since the probability of having an LoS channel is a function of the transceiver distance [6], it is intuitive to place the RIS in the middle to balance the probabilities of both users to have a LoS link to the RIS.

[4]The Rician fading is considered to account for the scattered multipath components besides the direct LoS path of the user-RIS channel [12].

Table I: Simulation Parameters

Parameter	Value
Carrier frequency	$f_c = 28$ GHz [6]
Bandwidth	$B = 1$ GHz
Waveguide/RIS height	$h = 3$ m [6]
Distance from origin to user's region	$d = 25$ m
Side length of user's region	$a = 10$ m
Equipment power consumption	$P_{\text{RE}} = P_{\text{UE},k} = 10$ dBm [22]
Amplifier efficiency	$\nu = 0.5$ [17]
path-loss parameter a	$a = 61.4$ [13]
path-loss parameter b	$b = 2$ [13]
RIS impairment severity	$\epsilon = 0.5$ [23]
Rician factor	$\mathcal{K} = 10$
Noise power	$\sigma^2 = -80$ dBm
Phase-shifter consumption	$P_{\text{ph-sh}} = 17.5$ mW [24]
Movement motor consumption	$P_{\text{mov},k} = 3$ W [20]
Pinching/release motor consumption	$P_{\text{pin},k} = 1.08$ W [21]

B. RIS-Assisted System

The overall energy efficiency of RIS-assisted communication system can be expressed as follows:

$$EE^{\text{RIS}} = \frac{B \cdot \sum_{k}^{K=2} R_k^{\text{RIS}}}{P_{\text{RIS}} + \sum_{k}^{K=2} (P_k + P_{\text{UE},k})}, \tag{15}$$

where P_{RIS} is the power dissipated by the RIS, which depends on the phase-shifter of the individual elements. Hence, P_{RIS} can be given as follows:

$$P_{\text{RIS}} = M P_{\text{ph-sh}}, \tag{16}$$

where $P_{\text{ph-sh}}$ is the power consumption of each phase shifter.

IV. Numerical Results

In this section, we numerically evaluate the performance of pinching antenna and RIS-assisted systems. To ensure accuracy, we employ Monte Carlo simulations with 10^4 realizations to verify the derived expressions for the pinching antenna and RIS communication scenarios. Unless stated otherwise, the simulation parameters are provided in Table I.

A. Hardware Impairments for Pinching Antennas and RIS

In our comparison, we further investigate the impact of hardware impairments on the performance of pinching antenna and RIS-assisted systems. To enrich the analysis, the following hardware impairments are considered

1) **Lossy pinching antenna:** In practice, the available transmit power P_k may not be fully coupled through the pinching antenna, leading to a power loss [6]. This effect is modeled by βP_k, where $\beta \in [0, 1]$ represents portion of the transmit power emitted by the pinching antenna.
2) **Lossy waveguide with end-feeder:** The dielectric waveguide exhibits a propagation loss of approximately 0.08 dB/m at 28 GHz [6], which can significantly affect signal strength over long distances. Moreover, a single feed point is located at one end of the waveguide is considered, i.e., at location $(-d-a, 0, h)$ as in Fig. 1(a), where we evaluate the performance of the user located at the far end of the waveguide feeder.
3) **Lossy waveguide with mid-feeder:** This scenario assumes that two co-located feed points are deployed at the center of the waveguide with 0.08 dB/m propagation loss [6], i.e., at location $(0, 0, h)$, which can send signals bidirectionally along the waveguide depending on the served user's location.
4) **RIS with phase noise per element:** Recall that θ_m is the optimal phase shift for coherent beamforming. However, due to hardware imperfections, the actual phase-shift applied by each element is $\tilde{\theta}_m = \theta_m + \hat{\theta}_m$, where $\hat{\theta}_m \sim \mathcal{U}[-\epsilon\pi, \epsilon\pi]$ represents the phase noise [23], $\mathcal{U}$ denotes the uniform distribution and ϵ measures the severity of the impairments at the RIS. Note that $\epsilon = 0$ corresponds to perfect phase adjustment (i.e., without phase noise), while $\epsilon = 1$ represents the worst-case scenario.

In Fig. 2(a), the spectral efficiency is plotted versus the number of reflecting elements of the RIS and compared with the performance of pinching antenna systems, considering the hardware impairments for both technologies as discussed earlier. It can be observed that as the number of RIS elements increases, the impact of hardware impairments becomes more prominent, indicating that large-scale RIS deployments may suffer from reduced efficiency due to these imperfections. For pinching antenna systems, the performance degradation caused by mid-feeder configuration and antenna loss case remains relatively close to the simulation curve of the ideal case. As expected, the worst performance is observed when the waveguide uses a single feeder located at one end, due to higher propagation losses. Interestingly, under this worst-case pinching antenna scenario, the RIS with phase-noise impairments requires approximately 7×10^4 reflecting elements to outperform pinching antenna setup. This number increases to around 8×10^4 elements to outperform the mid-feeder configuration and antenna loss case. Additionally, as discussed earlier, using the pinching antenna in a similar manner to RIS to perform communication over two time slots yields no performance gains. Finally, a good match between the closed-form expressions and the simulation results is achieved.

In Fig. 2(b), we investigate the spectral efficiency performance of pinching antennas and RIS when the horizontal distance between user's service regions increase. As expected, the single-feeder waveguide exhibits a sharper decline in performance compared to double-feeder waveguide as d increase. One can also observe that RIS is more susceptible to severe path loss, where the performance gap between the pinching-antenna and RIS increases significantly with d. This result shows the great flexibility of pinching-antenna systems to combat path loss, and demonstrates greater robustness to distance variation compared to RIS.

Fig. 2(c) illustrates the system energy efficiency as a function of transmit power (in dBm) for both the pinching antenna and RIS-assisted systems, considering hardware impairments. The results clearly demonstrate that the RIS-assisted system becomes highly inefficient in the mmWave band when compared to the significantly superior performance of the pinching antenna system, as illustrated in the figure. For instance, the pinching antenna system achieves a peak energy efficiency of

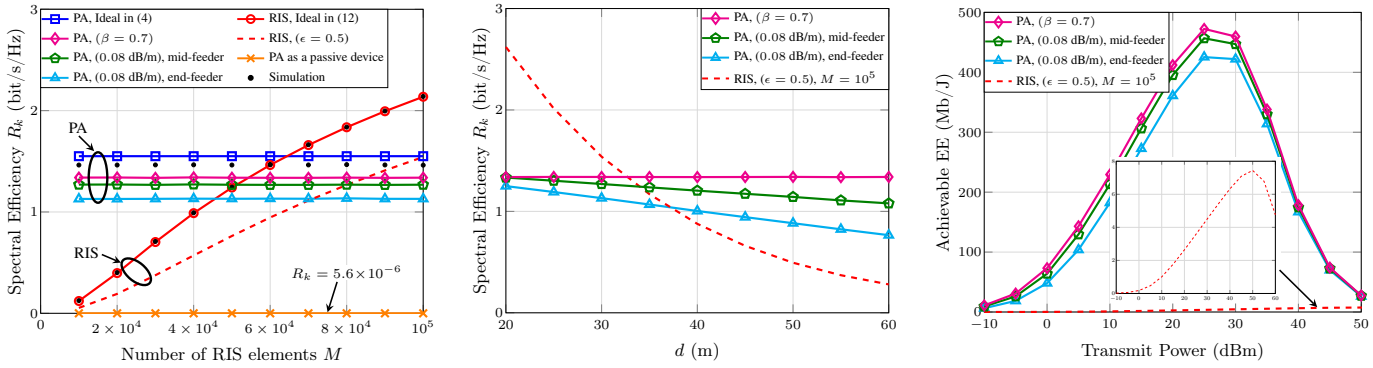

(a) Spectral efficiency vs RIS elements ($P_k = 15$ dBm). (b) Spectral efficiency vs distance ($P_k = 15$ dBm). (c) Energy efficiency vs transmit power.

Fig 2. Spectral and energy efficiency performance of pinching antenna systems (PA) and RIS-assisted systems in mmWave band.

approximately 480 Mb/J at a transmit power of 25 dBm. In contrast, RIS-assisted systems only reaches a peak of around 7 Mb/J at much higher transmit power of 50 dBm, which is not practical in many wireless communication scenarios. This performance deterioration of RIS is due to the need for a large number of elements (in the order of 10^4) to overcome the severe double path loss in mmWave frequencies.

V. Conclusions

We have compared the emerging pinching antenna systems with RIS-assisted systems in mmWave bands. The key observation is that RIS requires massive number of elements to be competitive with pinching antenna systems in terms of spectral efficiency, which severely impact the energy efficiency performance of RIS. Additionally, pinching antenna systems demonstrated greater robustness against hardware impairments and severe path loss, especially when the waveguide feeder point is placed at the center of the waveguide. An important direction for future research is the study of the coexistence between pinching antennas and RIS, which may offer complementary capabilities in next-generation wireless networks.

References

[1] M. Xiao *et al.*, "Millimeter wave communications for future mobile networks," *IEEE J. Sel. Areas Commun.*, vol. 35, no. 9, pp. 1909–1935, Sep. 2017.

[2] R. Flamini *et al.*, "Toward a heterogeneous smart electromagnetic environment for millimeter-wave communications: An industrial viewpoint," *IEEE Trans. Antennas Propag.*, vol. 70, no. 10, pp. 8898–8910, Oct. 2022.

[3] S. Rangan, T. S. Rappaport, and E. Erkip, "Millimeter-wave cellular wireless networks: Potentials and challenges," *Proc. IEEE*, vol. 102, no. 3, pp. 366–385, Mar. 2014.

[4] E. Basar *et al.*, "Wireless communications through reconfigurable intelligent surfaces," *IEEE Access*, vol. 7, pp. 116 753–116 773, Feb. 2019.

[5] H. O. Y. Suzuki and K. Kawai, "Pinching antenna: Using a dielectric waveguide as an antenna," *NTT DOCOMO Technical J.*, Jan. 2022.

[6] Z. Ding, R. Schober, and H. Vincent Poor, "Flexible-antenna systems: A pinching-antenna perspective," *IEEE Trans Commun.*, pp. 1–1, 2025.

[7] Z. Yang *et al.*, "Pinching antennas: Principles, applications and challenges," *arXiv preprint arXiv:2501.10753*, 2025.

[8] Y. Xu, Z. Ding, and G. K. Karagiannidis, "Rate maximization for downlink pinching-antenna systems," *IEEE Wireless Commun. Lett.*, vol. 14, no. 5, pp. 1431–1435, May 2025.

[9] S. A. Tegos, P. D. Diamantoulakis, Z. Ding, and G. K. Karagiannidis, "Minimum data rate maximization for uplink pinching-antenna systems," *IEEE Wireless Commun. Lett.*, vol. 14, no. 5, pp. 1516–1520, May 2025.

[10] K. Wang, Z. Ding, and R. Schober, "Antenna activation for NOMA assisted pinching-antenna systems," *IEEE Wireless Commun. Lett.*, vol. 14, no. 5, pp. 1526–1530, May 2025.

[11] Y. Qin, Y. Fu, and H. Zhang, "Joint antenna position and transmit power optimization for pinching antenna-assisted ISAC systems," *arXiv preprint arXiv:2503.12872*, 2025.

[12] M. Rahal *et al.*, "RIS-enabled NLoS near-field joint position and velocity estimation under user mobility," *IEEE J. Sel. Topics Signal Process.*, vol. 18, no. 4, pp. 633–645, May 2024.

[13] M. Cheng *et al.*, "Impact of finite-resolution precoding and limited feedback on rates of IRS based mmWave networks," *IEEE Trans. Veh. Technol.*, vol. 71, no. 5, pp. 5172–5186, May 2022.

[14] P. Wang *et al.*, "Intelligent reflecting surface-assisted millimeter wave communications: Joint active and passive precoding design," *IEEE Trans. Veh. Technol.*, vol. 69, no. 12, pp. 14 960–14 973, Dec. 2020.

[15] A. Rech *et al.*, "Clustering-based downlink scheduling of IRS-assisted communications with reconfiguration constraints," *IEEE Trans. Wireless Commun.*, vol. 23, no. 12, pp. 18 487–18 501, Dec. 2024.

[16] M. Samy, H. Al-Hraishawi, S. Chatzinotas, and B. Otteresten, "Outage performance of multiple hybrid active relays and RISs-assisted NOMA networks," *IEEE Wireless Commun. Lett.*, pp. 1–5, May 2024.

[17] E. Björnson, Ö. Özdogan and E. G. Larsson, "Intelligent reflecting surface versus decode-and-forward: How large surfaces are needed to beat relaying?" *IEEE Wireless Commun. Lett.*, vol. 9, no. 2, pp. 244–248, Feb. 2020.

[18] Y. Liu *et al.*, "Pinching-antenna systems (PASS): Architecture designs, opportunities, and outlook," 2025. [Online]. Available: https://arxiv.org/abs/2501.18409

[19] X. Wei *et al.*, "Mechanical power modeling and energy efficiency maximization for movable antenna systems," *arXiv preprint arXiv:2505.05914*, 2025.

[20] Faulhaber, "Stepper motors, series AM2224." [Online]. Available: https://www.faulhaber.com/en/products/series/am2224/

[21] Faulhaber, "Stepper motors, series AM1020." [Online]. Available: https://www.faulhaber.com/en/products/series/am1020/

[22] M. Samy *et al.*, "Beyond diagonal RIS-aided networks: Performance analysis and sectorization tradeoff," *IEEE Open J. Commun. Soc.*, vol. 6, pp. 302–315, 2025.

[23] X. Qian *et al.*, "Beamforming through reconfigurable intelligent surfaces in single-user MIMO systems: SNR distribution and scaling laws in the presence of channel fading and phase noise," *IEEE Wireless Commun. Lett.*, vol. 10, no. 1, pp. 77–81, 2021.

[24] E. V. P. Anjos, D. Schreurs, G. A. E. Vandenbosch, and M. Geurts, "A compact 26.5–29.5-GHz LNA-phase-shifter combo with 360° continuous phase tuning based on all-pass networks for millimeter-wave 5G," *IEEE Trans. Circuits Syst. I, Reg. Papers*, vol. 68, no. 9, pp. 3927–3940, Sep. 2021.